Anomalous diffusion of scaled Brownian tracers

Francisco J. Sevilla [1,*], Adriano Valdés-Gómez [2,3] and Alexis Torres-Carbajal [1]

[1]*Instituto de Física, Universidad Nacional Autónoma de México, P.O. Box 20-364, 01000 Ciudad de México, Mexico*

[2]*AI Factory at BBVA México*

[3]*Facultad de Ciencias, Universidad Nacional Autónoma de México, Alcaldía Coyoacán, C.P. 04510 Ciudad Universitaria, Ciudad de México, Mexico*

(Received 2 January 2024; accepted 29 May 2024; published 3 July 2024)

A model for anomalous transport of tracer particles diffusing in complex media in two dimensions is proposed. The model takes into account the characteristics of persistent motion that an active bath transfers to the tracer; thus, the model proposed here extends active Brownian motion, for which the stochastic dynamics of the orientation of the propelling force is described by scaled Brownian motion (sBm), identified by time-dependent diffusivity of the form $D_\beta \propto t^{\beta-1}$, $\beta > 0$. If $\beta \neq 1$, sBm is highly nonstationary and suitable to describe such nonequilibrium dynamics induced by complex media. In this paper, we provide analytical calculations and computer simulations to show that genuine anomalous diffusion emerges in the long-time regime, with a time scaling of the mean-squared displacement $t^{2-\beta}$, while ballistic transport t^2, characteristic of persistent motion, is found in the short-time regime. We also analyze the time dependence of the kurtosis, and the intermediate scattering function of the position distribution, as well as the propulsion autocorrelation function, which defines the effective persistence time.

DOI: 10.1103/PhysRevE.110.014113

I. INTRODUCTION

Anomalous diffusion refers to those transport processes whose mean-squared displacement (MSD) scales asymptotically as a power law with time, i.e.,

$$\langle \boldsymbol{x}^2(t)\rangle \sim t^\beta \tag{1}$$

with $\beta > 0$. The term subdiffusion is used for the cases where $0 < \beta < 1$, while superdiffusion denotes cases where $\beta > 1$. Normal diffusion is the term left for the traditional diffusion of a Brownian particle for which $\beta = 1$.

Depending on the specific mechanism that leads to anomalous transport of tracer particles in complex environments, if known, a specific mathematical model can be devised to describe the power-law time dependence of the MSD. Commonly, if the origin of the anomalous behavior is unclear, predictions of the timescaling of the MSD given by different models are fitted to the experimental results in order to obtain the values of the relevant parameters of the model. A standard approach to model the effects of complex environments on tracer motion is to implicitly incorporate them, in the form of complex noise, into a stochastic differential equation model (Langevin-like models) [1–3].

Recently, anomalous diffusion of tracer particles in complex media, particularly in nonequilibrium environments made of active particles (active baths) [1–5] or of viscoelastic fluid [6–8], has been observed. In these cases, the transport properties of the tracer particle mimic those of active motion, exhibiting highly *persistent* motion. Active or propelled particles are the name for those agents that locally transform, through complex mechanisms, the energy adsorbed from the environment into a variety forms of locomotion. Active Brownian motion is a simple stochastic model for active motion and is based in the overdamped motion of a Brownian particle subject to propelling force $v_0\hat{\boldsymbol{v}}(t)$, i.e.,

$$\frac{d}{dt}\boldsymbol{x}(t) = v_0\hat{\boldsymbol{v}}(t), \tag{2}$$

where v_0 is the constant propulsion speed, and $\hat{\boldsymbol{v}}(t) = (\cos\varphi(t), \sin\varphi(t))$ is the direction of propulsion, randomized by the fluctuations of the propelling mechanism; in the simplest case, these are modeled by rotational Brownian motion.

In this paper we consider the case in which the stochastic dynamics of the propelling direction of active Brownian particles is modeled by scaled Brownian motion. In contrast to the results reported in [9], where the dynamics of the propelling direction was modeled by fractional Brownian motion, here we show the emergence of genuine anomalous diffusion.

Scaled or geometric Brownian motion (sBm), is a nonstationary and nonergodic stochastic process $\chi_\beta(t)$ whose time evolution is given by the Langevin-like stochastic differential equation [10–13]

$$\frac{d}{dt}\chi_\beta(t) = \sqrt{2\beta K_\beta t^{\beta-1}}\xi(t), \tag{3}$$

where $\xi(t)$is Gaussian white noise, i.e., $\langle\xi(t)\rangle = 0$ and $\langle\xi(t)\xi(s)\rangle = \delta(t-s)$; K_β has units of $[\chi(t)]^2$ over $[\text{time}]^\beta$, which generalizes the meaning of the diffusion coefficient when $\beta = 1$, and $\chi(t)$ has units of length. Scaled Brownian motion has been considered in a variety of physical and nonphysical processes and it naturally provides a seemingly adequate description in the case of unbounded diffusion of anomalous diffusion since for $0 < \beta < 1$ the amplitude of

*Contact author: fjsevilla@fisica.unam.mx

fluctuations in Eq. (3) extinguishes with time, giving rise to subdiffusion $\langle \chi^2(t)\rangle \propto t^\beta$, while superdiffusion is observed if $1 < \beta$ when the fluctuation grows without limit with time.

The associated Fokker-Planck equation for the probability density, $P(\chi, t)$, of finding the outcome χ at time t for $\chi_\beta(t)$, is given by Batchelor's equation [11,14,15]

$$\frac{\partial}{\partial t}P_\beta(\chi, t) = D_{K,\beta}(t)\frac{\partial^2}{\partial \chi^2}P_\beta(\chi, t) \tag{4}$$

where $D_{K,\beta}(t) = \beta K_\beta t^{\beta-1}$ is the time-dependent diffusion coefficient. sBm has been used to describe anomalous diffusion, for instance in the anomalous diffusion properties of fluorescently tagged gold beads in the cytoplasm and the nucleus of living cells [16], in the self-diffusion in granular gases [17], in numerical simulations of fluorescence photobleaching recovery experiments [18], or as a model to fit parameters in fluorescence correlation spectroscopy [19]. Different studies have shown that the statistical properties of sBm give rise to a variety of nontrivial effects [20–25], particularly under conditions that exacerbate them, for instance, under conditions of confinement [12,26] or when particles move on manifolds [27].

In Sec. II we detail the mathematical model for the analysis, namely active Brownian particles driven by scaled Brownian motion. We give the model as stochastic differential equations from which ensembles of trajectories are obtained through numerical solutions. We also provide the corresponding Fokker-Planck equation for the probability density of finding a particle at position $\boldsymbol{x}$ and propelled in the direction $\hat{\boldsymbol{v}}$ at time t, from which analytical results are obtained. In Sec. III we focus our analysis on the reduced probability density which is independent of the propelling direction, from which approximated results for the intermediate scattering function (ISF) and kurtosis are obtained. Remarkably the mean-squared displacement and propulsion autocorrelation function (PACF) are obtained in the exact same manner. We conclude in Sec. IV.

II. THE MODEL

We consider a particle that is propelled in a two-dimensional domain with constant propulsion speed v_0 along the direction $\hat{\boldsymbol{v}}(t) = (\cos\varphi_\beta(t), \sin\varphi_\beta(t))$, $\varphi_\beta(t)$ being the angle between the direction of motion and the horizontal axis. Active fluctuations affect the rotational dynamics leading to rotational diffusion of the propelling "force," which in this paper is modeled by sBm. The overdamped dynamics of an active Brownian particle follow from the Langevin equations [28,29]

$$\frac{d}{dt}\boldsymbol{x}(t) = v_0\,\hat{\boldsymbol{v}}(t), \tag{5a}$$

$$\frac{d}{dt}\varphi_\beta(t) = \sqrt{2D_{R,\beta}(t)}\,\xi(t), \tag{5b}$$

where $\boldsymbol{x}(t) = (x_1(t), x_2(t))$ denotes the particle position and with $0 < \beta$. $\xi(t)$ in Eq. (5b) is Gaussian white noise, $\langle\xi\rangle = 0$, $\langle\xi(t)\xi(s)\rangle = \delta(t-s)$, and $D_{R,\beta}(t) = \beta R_\beta t^{\beta-1}$ with R_β a constant with units of $1/[\text{time}]^\beta$ that gives a measure of the fluctuations at a given time. Standard rotational Brownian motion is recovered in the case $\beta = 1$. We introduce the length $l = v_0/R_\beta^{1/\beta}$ as the distance traveled by a particle during the time $R_\beta^{-1/\beta}$.

The Fokker-Planck equation for the probability density $P(\boldsymbol{x}, \varphi, t) \equiv \langle\delta[\boldsymbol{x} - \boldsymbol{x}(t)]\delta[\varphi - \varphi_\beta(t)]\rangle$ corresponding to Eqs. (5) is given by

$$\frac{\partial}{\partial t}p_\beta(\boldsymbol{x}, \varphi, t) + v_0\nabla\cdot\,\hat{\boldsymbol{v}}\,p_\beta(\boldsymbol{x}, \varphi, t) = D_{R,\beta}(t)\frac{\partial^2}{\partial\varphi^2}p_\beta(\boldsymbol{x}, \varphi, t), \tag{6}$$

which corresponds to active Brownian motion driven by sBm dynamics.

III. THE REDUCED PROBABILITY DISTRIBUTION $p_\beta(\boldsymbol{x}, t)$

We now focus our analysis on the reduced distribution of the particle positions, i.e., we focus on the probability density function of finding a particle at position $\boldsymbol{x}$ at time t regardless of the direction of motion φ. We consider as initial distribution the one that corresponds to a pulse at the origin with vanishing probability current, i.e., $p_\beta(\boldsymbol{x}, \varphi, 0) = \delta(\boldsymbol{x})/2\pi$.

We solve numerically Eqs. (5) for an ensemble of $N = 2.3\times10^5$ particles up to times $t = 10^4\,R_\beta^{-1/\beta}$, using a discretization time step $\Delta t = 10^{-3}\,R_\beta^{-1/\beta}$ in an implementation of the Euler-Maruyama method. This is straightforwardly applied to Eq. (5b) to obtain $\varphi_\beta(t)$; with this a simple Euler update scheme is used to compute $\boldsymbol{x}(t)$. The positions of the particles in the ensemble are shown in Fig. 1 at time $t = 10\,R_\beta^{-1/\beta}$; additionally, five typical trajectories are shown to exhibit the stochastic dynamics for $\beta = 0.2$, 0.4, 0.6, 0.8, 1.0, 1.2, 1.4, 1.6, and 1.8.

First, we resort to the Fourier transform of the spatial variables of Eq. (6), i.e., $\boldsymbol{x} = (x_1, x_2) \longrightarrow \boldsymbol{k} = (k_1, k_2)$:

$$\frac{\partial}{\partial t}\hat{p}_\beta(\boldsymbol{k}, \varphi, t) + iv_0\,\hat{\boldsymbol{v}}\cdot\boldsymbol{k}\,\hat{p}_\beta(\boldsymbol{k}, \varphi, t) = D_{R,\beta}(t)\frac{\partial^2}{\partial\varphi^2}\hat{p}_\beta(\boldsymbol{k}, \varphi, t), \tag{7}$$

where $\hat{f}(\boldsymbol{k}) = \int d^2x\, e^{-i\boldsymbol{k}\cdot\boldsymbol{x}}\,f(\boldsymbol{x})$ denotes the Fourier transform of $f(\boldsymbol{x})$ and $\boldsymbol{k} = (k_x, k_y)$ denotes the Fourier wave vector. We consider the series expansion

$$\hat{p}_\beta(\boldsymbol{k}, \varphi, t) = \frac{1}{2\pi}\sum_{n=-\infty}^{\infty}\hat{q}_\beta^{(n)}(\boldsymbol{k}, t)\,e^{-R_\beta t^\beta n^2}e^{in\varphi}, \tag{8}$$

where $\{e^{-R_\beta t^\beta n^2}e^{in\varphi}\}$ with n an integer is the set of independent solutions of the equation

$$\frac{\partial}{\partial t}\Phi_\beta(\varphi, t) = D_{R,\beta}(t)\frac{\partial^2}{\partial\varphi^2}\Phi_\beta(\varphi, t). \tag{9}$$

The coefficients of the expansion (8) are obtained using the standard orthogonality relation among the Fourier basis functions $\{e^{in\varphi}\}$, explicitly

$$\hat{q}_\beta^{(n)}(\boldsymbol{k}, t) = e^{R_\beta t^\beta n^2}\int_{-\pi}^{\pi}d\varphi\,\hat{p}_\beta(\boldsymbol{k}, \varphi, t)e^{-in\varphi}. \tag{10}$$

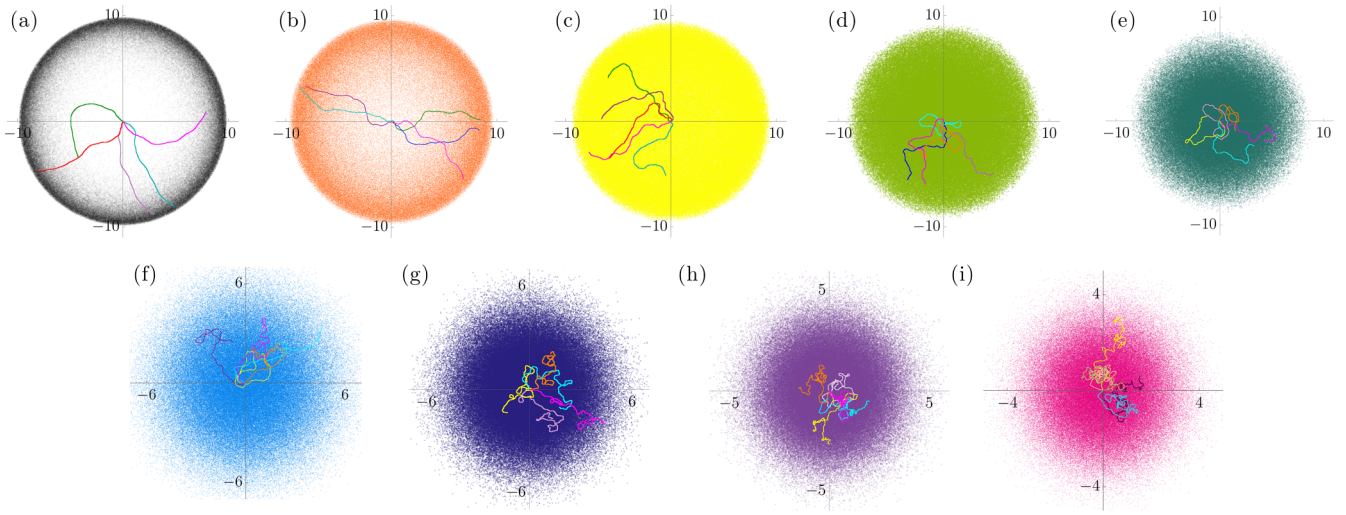

FIG. 1. Snapshots of the positions of an ensemble of 2.3×10^5 particles at time $t = 10\,R_\beta^{-1/\beta}$ are shown for $\beta = 0.2$ (a), 0.4 (b), 0.6 (c), 0.8 (d), 1.0 (e), 1.2 (f), 1.4 (g), 1.6 (h), and 1.8 (i). In each case, five typical trajectories are traced during the time interval $[0, 10R_\beta^{1/\beta}]$, all of them starting at the origin of coordinates and initial directions chosen uniformly and random in $[0, \pi]$.

From this we have

$$\hat{q}_\beta^{(0)}(\boldsymbol{k}, t) = \int_{-\pi}^{\pi} d\varphi\, \hat{p}_\beta(\boldsymbol{k}, \varphi, t) \tag{11}$$

which corresponds to the self-part or coherent part of the ISF. This is obtained from numerical simulations and shown in Fig. 2 for small wave-vector number $kl = 0.1$ [Fig. 2(a)], intermediate $kl = 1.0$ [Fig. 2(b)], and large wave-vector number $kl = 10.0$ [Fig. 2(c)]; in all cases, the ballistic short-time behavior ($\hat{p}_\beta \approx 1$) is clearly observed.

In the case $kl = 10$, ISF characterizes the particle position distribution at short length scales. At short times, it relaxes in the same manner independently of the value of β. In this regime, particle distributions are all alike, as the one shown in Fig. 1(a), corresponding to ballistic propagation. After times of the order of $tR_\beta^{1/\beta} \gtrsim 1$, relaxation of the ISF depends on β as shown by the long-lasting oscillations the smaller β is. For the cases for which the wave-vector number is of the order of or smaller than l^{-1}, $kl \lesssim 1$ [$kl = 1.0$ and 0.1 are shown in Figs. 2(b) and 2(a), respectively], it is possible to identify the effects of the different values of β in the intermediate-time regimes, i.e., the ISF relaxation distinguishes among the distinct patterns of propagation induced by the different sBm exponent β. For $kl = 1.0$ in Fig. 2(b) the ISF oscillates, decaying to zero faster if $\beta \lesssim 1.0$; instead it decays slowly and monotonically when $\beta > 1$, meaning that the corresponding

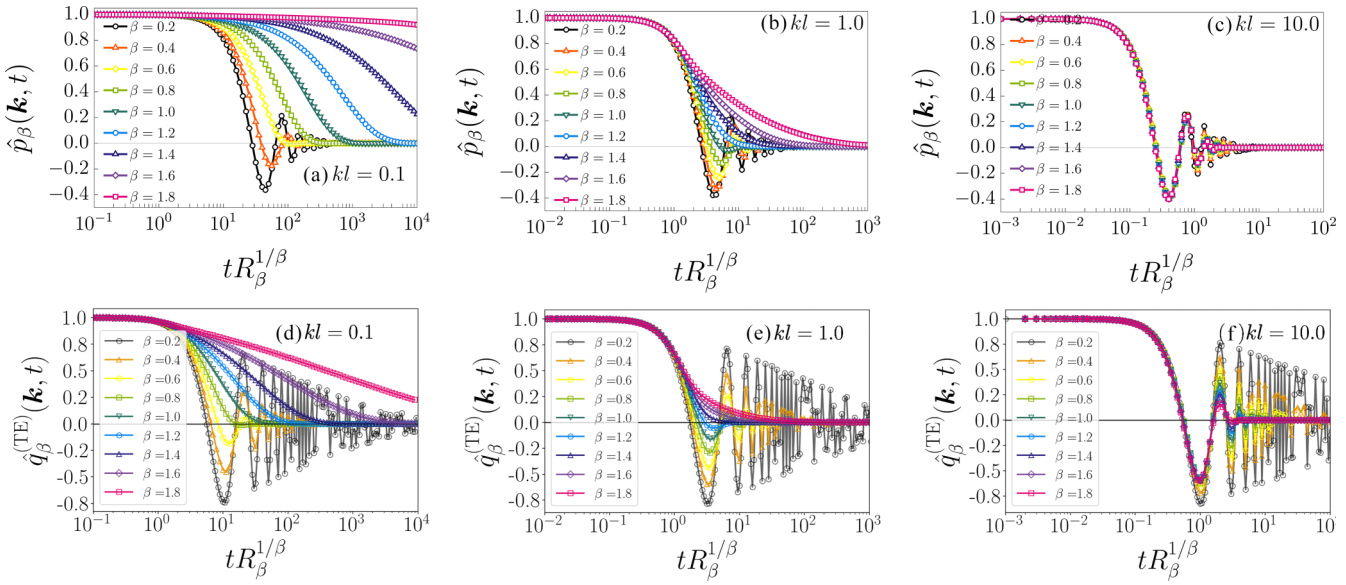

FIG. 2. The time dependence of the intermediate scattering function. Top row: Results obtained from numerical simulations, $\hat{p}_\beta(\boldsymbol{k}, t)$, for dimensionless wave vectors $kl = 0.1$ (a), 1.0 (b), and 10.0 (c). Bottom row: Results obtained from the numerical integration of Eq. (17), $\hat{q}_\beta^{(\mathrm{TE})}(\boldsymbol{k}, t)$, for dimensionless wave vectors $kl = 0.1$ (d), 1.0 (e), and 10.0 (f).

relaxation time increases. These features are more noticeable the smaller the values of kl are. In Fig. 2(a) the case $kl = 0.1$ is shown; now the oscillating decay of the ISF is observed for $\beta \lesssim 0.6$ and monotonically decaying ISFs for $\beta > 0.6$. Similar characteristics have been reported in the case $\beta = 1$ in standard active Brownian motion [30,31]. Figures 2(d)–2(f) also include approximate results for the ISF computed from a generalization of the telegrapher equation, which is discussed in the next section.

The moments of $p_\beta(\boldsymbol{x}, t)$ are of interest and can be obtained from its characteristic function $\hat{p}_\beta(\boldsymbol{k}, t) = \hat{q}_\beta^{(0)}(\boldsymbol{k}, t)$ as follows:

$$\langle x_1^{m_1} x_2^{m_2} \rangle = \left[\left(-i \frac{\partial}{\partial k_1} \right)^{m_1} \times \left(-i \frac{\partial}{\partial k_2} \right)^{m_2} \hat{q}_\beta^{(0)}(\boldsymbol{k}, t) \right]_{\substack{k_1=0 \\ k_2=0}}. \tag{12}$$

After substitution of Eq. (8) into Eq. (7) and after use of the orthogonality of the Fourier basis functions, we get the following set of coupled ordinary differential equations for the nth coefficient of the expansion $\hat{q}_\beta^{(n)}(\boldsymbol{k}, t)$:

$$\frac{d}{dt}\hat{q}_\beta^{(n)}(\boldsymbol{k}, t) = -i\frac{v_0}{2}k\left[e^{-i\theta}e^{-R_\beta t^\beta(1-2n)}\,\hat{q}_\beta^{(n-1)}(\boldsymbol{k}, t) + e^{i\theta}e^{-R_\beta t^\beta(1+2n)}\,\hat{q}_\beta^{(n+1)}(\boldsymbol{k}, t)\right], \tag{13}$$

with θ and $k = |\boldsymbol{k}|$ defined through the relations $k_1 \pm ik_2 \equiv ke^{\pm i\theta} \equiv k_\pm$ and the initial conditions $\hat{q}_\beta^{(n)}(\boldsymbol{k}, 0) = \delta_{n,0}$ which correspond to the initial distribution $P_\beta(\boldsymbol{x}, \varphi, 0) = \delta(\boldsymbol{x})/2\pi$, $\delta_{n,m}$ being the standard Kronecker delta.

A. The $\hat{q}_\beta^{(\pm 1)}$ approximation: The telegrapher equation with time-dependent relaxation coefficient

We can close the coupled Eq. (13) up to $\hat{q}_\beta^{(\pm 1)}(\boldsymbol{k}, t)$, disregarding, as a first approximation, all coefficients $\hat{q}_\beta^{(n)}(\boldsymbol{k}, t)$ with $|n| > 1$ [32,33]. This approximation is expected to be appropriate in the long-time regime since high Fourier modes in the expansion (8) are negligible in that limit. However, for $0 < \beta < \frac{1}{2}$, this is not the case due to the slow dynamics. Notwithstanding this, the exact time dependence of the MSD is obtained from this, as is shown afterwards. We have that in this approximation

$$\frac{\partial}{\partial t}\hat{q}_\beta^{(1)}(\boldsymbol{k}, t) = -i\frac{v_0}{2}ke^{-i\theta}e^{R_\beta t^\beta}\hat{q}_\beta^{(0)}(\boldsymbol{k}, t), \tag{14a}$$

$$\frac{\partial}{\partial t}\hat{q}_\beta^{(0)}(\boldsymbol{k}, t) = -i\frac{v_0}{2}ke^{-R_\beta t^\beta}\left[e^{-i\theta}\hat{q}_\beta^{(-1)}(\boldsymbol{k}, t) + e^{i\theta}\hat{q}_\beta^{(1)}(\boldsymbol{k}, t)\right], \tag{14b}$$

$$\frac{\partial}{\partial t}\hat{q}_\beta^{(-1)}(\boldsymbol{k}, t) = -i\frac{v_0}{2}ke^{i\theta}e^{R_\beta t^\beta}\hat{q}_\beta^{(0)}(\boldsymbol{k}, t). \tag{14c}$$

The $\hat{q}_\beta^{(0)}(\boldsymbol{k}, t)$ in Eq. (11) must be distinguished from the corresponding solution of Eqs. (14), which is an approximation of the former, referred to as $\hat{q}_\beta^{(\mathrm{TE})}(\boldsymbol{k}, t)$. This is given by

$$\frac{\partial}{\partial t}\hat{q}_\beta^{(\mathrm{TE})}(\boldsymbol{k}, t) = -\frac{v_0^2}{2}k^2e^{-R_\beta t^\beta}\int_0^t ds\, e^{R_\beta s^\beta}\hat{q}_\beta^{(\mathrm{TE})}(\boldsymbol{k}, s), \tag{15}$$

with $k^2 = k_1^2 + k_2^2$. After inverting the Fourier transform, we obtain the generalized diffusion equation

$$\frac{\partial}{\partial t}q_\beta^{(\mathrm{TE})}(\boldsymbol{x}, t) = \frac{v_0^2}{2}\int_0^t ds\,\gamma(t; s)\nabla^2 q_\beta^{(\mathrm{TE})}(\boldsymbol{x}, s), \tag{16}$$

where the memory function $\gamma(t; s) = e^{-R_\beta(t^\beta - s^\beta)}$ is not time-translationally invariant, a characteristic that emerges from the inherently nonstationarity of the sBm process.

After taking the derivative with respect to time we get, equivalently,

$$\frac{\partial^2}{\partial t^2}\hat{q}_\beta^{(\mathrm{TE})}(\boldsymbol{k}, t) + D_{R,\beta}(t)\frac{\partial}{\partial t}\hat{q}_\beta^{(\mathrm{TE})}(\boldsymbol{k}, t) = -\frac{v_0^2}{2}k^2\hat{q}_\beta^{(\mathrm{TE})}(\boldsymbol{k}, t), \tag{17}$$

which corresponds to a damped harmonic oscillator with time-dependent damping coefficient $D_{R,\beta}(t)$, whose inverse Fourier transform is identified with the telegrapher's equation with time-dependent relaxation coefficient $D_{R,\beta}(t)$:

$$\frac{\partial^2}{\partial t^2}q_\beta^{(\mathrm{TE})}(\boldsymbol{x}, t) + D_{R,\beta}(t)\frac{\partial}{\partial t}q_\beta^{(\mathrm{TE})}(\boldsymbol{x}, t) = \frac{v_0^2}{2}\nabla^2 q_\beta^{(\mathrm{TE})}(\boldsymbol{x}, t). \tag{18}$$

The differential equations that determine the time dependence of the moments of $q_\beta^{(\mathrm{TE})}(\boldsymbol{x}, t)$ can be obtained by using Eq. (15), but with $q_\beta^{(\mathrm{TE})}(\boldsymbol{x}, t)$ instead of $q_\beta^{(0)}(\boldsymbol{x}, t)$.

In Figs. 2(d)–2(f), the time dependence of the ISF obtained from the numerical solution of the telegrapher equation with time-dependent relaxation coefficient (17) is shown for different values of the dimensionless wave vector kl and different scaling parameter β. The results are qualitatively in good agreement with those discussed in the previous section. The main differences with respect to the exactly computed cases [Figs. 2(a)–2(c)] are that relaxation times increase by orders of magnitude and oscillation amplitudes become larger for β ($\lesssim 0.5$); when the approximated ISF decays monotonically, the decaying is faster than in the exact case. This analysis elucidates the importance of the higher Fourier modes left aside in the approximation (14). Notwithstanding this, the approximation made in (14) leads to the exact time dependence of the MSD as discussed in the following section.

B. The mean-squared displacement

The diffusive transport of the particle is generically characterized by the second moment or mean-squared displacement of the position distributions $p_\beta(\boldsymbol{x}, t)$ and $\langle \boldsymbol{x}^2(t) \rangle = \int d^2x\, \boldsymbol{x}^2 p_\beta(\boldsymbol{x}, t)$ and, according to Eqs. (12) and (11), is given by

$$\langle \boldsymbol{x}^2(t) \rangle_{p_\beta} = \langle x_1^2(t) \rangle_{p_\beta} + \langle x_2^2(t) \rangle_{p_\beta} = -\left[\left(\frac{\partial^2}{\partial k_1^2} + \frac{\partial^2}{\partial k_2^2} \right) \hat{q}_\beta^{(0)}(\boldsymbol{k}, t) \right]_{\substack{k_1=0 \\ k_2=0}}. \tag{19}$$

After applying the differential operator of the last equation to the Fourier transform of the generalized diffusion equation (15), the approximation $\hat{q}_\beta^{(0)}(\boldsymbol{k}, t) \approx \hat{q}_\beta^{(\mathrm{TE})}(\boldsymbol{k}, t)$ leads

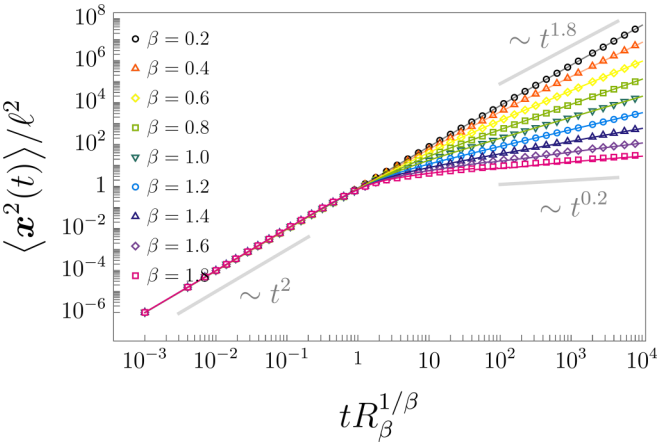

FIG. 3. Time dependence of the dimensionless mean-squared displacement $\langle \boldsymbol{x}^2(t)\rangle/\ell^2$, $\ell = v_0/R_\beta^{1/\beta}$ being the *persistence length*. Symbols show the exact result $\langle \boldsymbol{x}^2(t)\rangle$ from our numerical analysis, while continuous lines mark the analytical expression $\langle \boldsymbol{x}^2(t)\rangle_{\rm TE}$ (21) obtained from the $\hat{q}_\beta^{(\pm1)}$ approximation. The agreement is remarkable.

to the result

$$\frac{d}{dt}\langle \boldsymbol{x}^2(t)\rangle_{\rm TE} = 2v_0^2 e^{-R_\beta t^\beta}\int_0^t ds\, e^{R_\beta s^\beta}, \tag{20}$$

from which we get straightforwardly that

$$\langle \boldsymbol{x}^2(t)\rangle_{\rm TE} = 2v_0^2\int_0^t ds\, e^{-R_\beta s^\beta}\int_0^s ds_1\, e^{R_\beta s_1^\beta}, \tag{21}$$

where we have made explicit the initial condition $\langle \boldsymbol{x}^2(0)\rangle_{\rm TE} = 0$. This is one of the main results of our analysis. Expression (21) is evaluated numerically for $\beta = 0.2$, 0.4, 0.6, 0.8, 1.0, 1.2, 1.4, 1.6, and 1.8 and shown in Fig. 3 (solid lines) and compared with the exact results obtained from the numerical analysis of the trajectories ensemble obtained from integration of Eqs. (5) (symbols). The agreement is remarkable, corroborating that $\hat{q}_\beta^{\rm (TE)}(\boldsymbol{k}, t)$ gives the exact time dependence of the mean-squared displacement.

Although not evident at first a glance, analytical Eq. (21) masks a crossover between ballistic transport at the short-time regime $\langle \boldsymbol{x}^2(t)\rangle \approx v_0^2 t^2$ and anomalous diffusion $\langle \boldsymbol{x}^2(t)\rangle \sim t^{2-\beta}$ in the long-time one (see Fig. 3). This transition can be seen from the following heuristic argument. By taking the time derivative of Eq. (20) we get

$$\frac{d^2}{dt^2}\langle \boldsymbol{x}^2(t)\rangle_{\rm TE} + D_{R,\beta}(t)\frac{d}{dt}\langle \boldsymbol{x}^2(t)\rangle_{\rm TE} = 2v_0^2. \tag{22}$$

In the short-time regime, i.e., to times up to the order of $R_\beta^{1/\beta}$, the effects of noise expressed in the second term of Eq. (17) are negligible compared with the coherent term expressed by the second-order time derivative, and thus we disregard it from Eq. (22) to get approximately

$$\frac{d^2}{dt^2}\langle \boldsymbol{x}^2(t)\rangle_{\rm TE} = 2v_0^2, \tag{23}$$

whose solution with the corresponding initial conditions is $\langle \boldsymbol{x}^2(t)\rangle_{\rm TE} = v_0^2 t^2$. Analogously, in the long-time regime, the coherent motion described by the second-order time derivative becomes negligible with respect to the effects of fluctuations; thus we have that approximately

$$D_{R,\beta}(t)\frac{d}{dt}\langle \boldsymbol{x}^2(t)\rangle_{\rm TE} = 2v_0^2 \tag{24}$$

which yields $\langle \boldsymbol{x}^2(t)\rangle_{\rm TE} = \frac{2v_0^2}{R_\beta\beta(2-\beta)}t^{2-\beta}$.

A series expansion in powers of $R_\beta^{1/\beta}t$ can be obtained by using the series expansion of the stretched exponentials in Eq. (20). After carrying out the integrals, we get

$$\langle \boldsymbol{x}^2(t)\rangle_{\rm TE} = v_0^2 t^2\sum_{n,m=0}^{\infty}\frac{2(-1)^n(R_\beta t^\beta)^{n+m}}{n!\,m!(\beta m+1)[\beta(n+m)+2]} \tag{25}$$

which clearly leads to the ballistic transport when $R_\beta^{1/\beta}t \ll 1$. Conversely, an asymptotic expansion of the integral in (20) can be obtained after using the change of variable $s^\beta = t^\beta - R_\beta z$; thus, it can be written as

$$e^{R_\beta t^\beta}\frac{t^{1-\beta}}{R_\beta\beta}\int_0^{R_\beta t^\beta} dz\Big(1-\frac{z}{R_\beta t^\beta}\Big)^{1/\beta-1}e^{-z}.$$

Therefore, in the limit $R_\beta t^\beta \to \infty$ we have

$$\int_0^t ds\, e^{R_\beta s^\beta} \sim e^{R_\beta t^\beta}\frac{t^{1-\beta}}{R_\beta\beta}\left[1+O\Big(\frac{1}{R_\beta t^\beta}\Big)\right]. \tag{26}$$

By retaining the leading term in the asymptotic expansion, we substitute it into Eq. (20), and after integration we obtain

$$\langle \boldsymbol{x}^2(t)\rangle_{\rm TE} \sim \frac{2v_0^2}{R_\beta\beta(2-\beta)}t^{2-\beta} \tag{27}$$

as mentioned previously.

C. The kurtosis

The kurtosis of the bivariate distribution $p_\beta(\boldsymbol{x};t)$ is given by [34]

$$\kappa_\beta(t) = \langle[(\boldsymbol{x}(t)-\langle\boldsymbol{x}(t)\rangle)\Sigma^{-1}(\boldsymbol{x}(t)-\langle\boldsymbol{x}(t)\rangle)^{\rm T}]^2\rangle, \tag{28}$$

where $\boldsymbol{x}^{\rm T}$ denotes a column vector, the transpose of the row vector $\boldsymbol{x} = (x_1, x_2)$, and Σ is the 2×2 matrix defined by the average of the dyadic product $[\boldsymbol{x}(t)-\langle\boldsymbol{x}(t)\rangle]^{\rm T}\cdot[\boldsymbol{x}(t)-\langle\boldsymbol{x}(t)\rangle]$. It can be shown that, due to the invariance of $p_\beta(\boldsymbol{x},t)$ under spatial rotations, the kurtosis (28) reduces to

$$\kappa_\beta(t) = \frac{\langle x_1^4(t)\rangle}{\langle x_1^2(t)\rangle^2} + \frac{\langle x_2^4(t)\rangle}{\langle x_2^2(t)\rangle^2} + \frac{2\langle x_1^2(t)\,x_2^2(t)\rangle}{\langle x_1^2(t)\rangle\langle x_2^2(t)\rangle}. \tag{29}$$

Each moment involved can be computed by use of the formula (12). The moments in the denominators are the squares of the second moments computed in the calculation of the MSD. The exact fourth-order moments are given by

$$\langle x_i^4(t)\rangle_{p_\beta} = \left[\frac{\partial^4}{\partial k_i^4}\hat{q}_\beta^{(0)}(\boldsymbol{k},t)\right]_{\substack{k_1=0\\k_2=0}},\ (i=1,2), \tag{30a}$$

$$\langle x_1^2(t)\,x_2^2(t)\rangle_{p_\beta} = \left[\frac{\partial^4}{\partial k_1^2\partial k_2^2}\hat{q}_\beta^{(0)}(\boldsymbol{k},t)\right]_{\substack{k_1=0\\k_2=0}}. \tag{30b}$$

In Fig. 4 the exact time dependence of $\kappa_\beta(t)$, obtained from our numerical analysis, is shown (symbols) for different values of β ranging from 0.2 to 1.8. The short-time regime

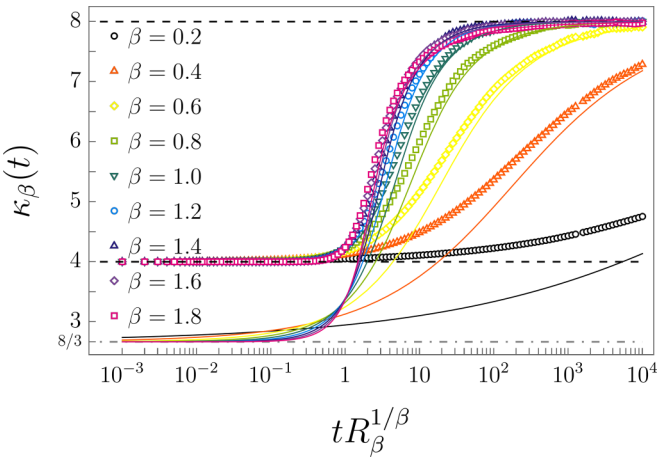

FIG. 4. Time dependence of the kurtosis of $p_\beta(\boldsymbol{x}, t)$ as defined in Eq. (28). Symbols mark the result from the ensemble average of the trajectories obtained from numerical simulations for $\beta = 0.2$, 0.4, 0.6, 0.8, 1.0, 1.2, 1.4, 1.6, and 1.8. Solid lines refer to the approximated result given in Eq. (32).

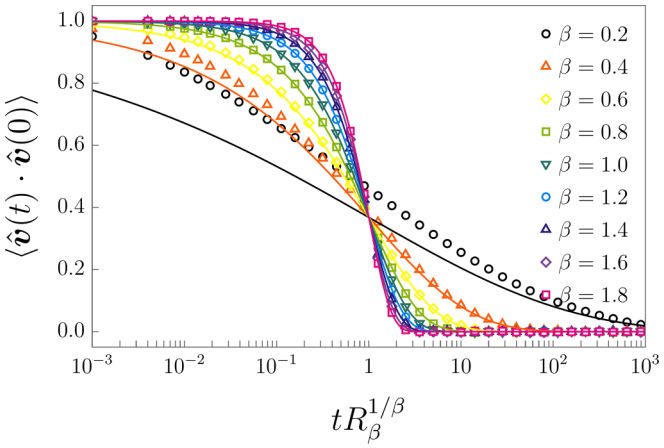

FIG. 5. Velocity autocorrelation function $\langle \hat{\boldsymbol{v}}(t) \cdot \hat{\boldsymbol{v}}(0) \rangle$. The symbols mark the exact results obtained from numerical simulations for $\beta = 0.2$, 0.4, 0.6, 0.8, 1.0, 1.2, 1.4, 1.6, and 1.8. Solid lines indicate the analytical formula $e^{-R_\beta t^\beta}$.

corresponds to a distribution of particle that propagates from the origin uniformly in all directions at speed v_0; at time t the particles are distributed around a "ring" of radius $v_0 t$; see for instance Fig. 1(a), which has kurtosis 4 transiting to the value 8, characteristic of a Gaussian in the long-time regime.

Differential equations for the fourth moments in the $\hat{q}_\beta^{(\pm 1)}$ approximation can be derived after applying the fourth-order derivatives in Eqs. (30) to Eq. (15); after some rearrangements, we get

$$\frac{d^2}{dt^2}\langle x_i^4(t)\rangle_{\rm TE} + D_{R,\beta}(t)\frac{d}{dt}\langle x_i^4(t)\rangle_{\rm TE} = 6v_0^2\langle x_i^2(t)\rangle_{\rm TE} \tag{31a}$$

and

$$\frac{d^2}{dt^2}\langle x_1^2(t)x_2^2(t)\rangle_{\rm TE} + D_{R,\beta}(t)\frac{d}{dt}\langle x_1^2(t)x_2^2(t)\rangle_{\rm TE} = v_0^2\big[\langle x_1^2(t)\rangle_{\rm TE} + \langle x_2^2(t)\rangle_{\rm TE}\big], \tag{31b}$$

whose solutions lead to the time dependence of the kurtosis in the $\hat{q}_\beta^{(\pm 1)}$ approximation

$$\kappa_{\beta,{\rm TE}}(t) = 16\frac{\int_0^t ds\, e^{-R_\beta s^\beta}\int_0^s ds_1\, e^{R_\beta s_1^\beta}\int_0^{s_1} ds_2\, e^{-R_\beta s_2^\beta}\int_0^{s_2} ds_3\, e^{R_\beta s_3^\beta}}{\big[\int_0^t ds\, e^{-R_\beta s^\beta}\int_0^s ds_1\, e^{R_\beta s_1^\beta}\big]^2}. \tag{32}$$

In contrast to the exact result in the short-time regime, $\kappa_\beta(t) \approx 4$, the $\hat{q}_\beta^{(\pm 1)}$ approximation yields a value $\kappa_{\beta,{\rm TE}} = \frac{8}{3} \approx 2.667$. Thus, failing to give the correct description in the short-time regime, however, in the long-time regime the approximation agrees well with exact time dependence. This is corrected by taking into consideration the next higher Fourier modes $\hat{q}_\beta^{(\pm 2)}$ in Eq. (13) as is shown in the Appendix.

D. The velocity autocorrelation function

The nonstationary fluctuations of sBm induce a relaxation of the PACF $\langle \hat{\boldsymbol{v}}(t) \cdot \hat{\boldsymbol{v}}(0)\rangle$ in the form of a stretched exponential, i.e.,

$$\langle \hat{\boldsymbol{v}}(t) \cdot \hat{\boldsymbol{v}}(0)\rangle = e^{-R_\beta t^\beta}, \tag{33}$$

which measures the persistence of active motion induced by sBm. Equation (33) was obtained by noticing that $\langle \hat{\boldsymbol{v}}(t) \cdot \hat{\boldsymbol{v}}(0)\rangle = \langle \cos[\varphi(t) - \varphi(0)]\rangle$ and using $\Phi(\varphi, t|\varphi', 0) = \frac{1}{2\pi}\sum_{n=0}^\infty e^{-R_\beta t^\beta n^2} e^{in(\varphi-\varphi')}$, the solution of Eq. (9) with initial distribution $\Phi(\varphi, 0|\varphi(0), 0) = \delta[\varphi - \varphi(0)]$. In the case $\beta = 1$, the simple exponential relaxation is recovered and R_1 is recognized with the rotational diffusion of standard active Brownian motion, that defines the persistence time $\tau_1 = \int_0^\infty dt\, e^{-R_1 t} = R_1^{-1}$. For $\beta \neq 1$ we have, analogously, $\tau_\beta = \int_0^\infty dt\, e^{-R_\beta t^\beta} = \Gamma(1+\beta^{-1})R_\beta^{-\beta^{-1}}$; this decreases monotonically with β being larger than R_1^{-1} for $0 < \beta < 1$ and smaller for $1 < \beta < 2$, implying the origin of the anomalous transport observed.

In Fig. 5 the PACF is shown from the numerical analysis (symbols) as a function of the dimensionless time $tR_\beta^{1/\beta}$ for $\beta = 0.2$ (dark circles), 0.4 (light up triangles), 0.6 (light diamonds), 0.8 (light squares), 1.0 (dark down triangles), 1.2 (light circles), 1.4 (dark up triangles), 1.6 (dark diamonds), and 1.8 (dark squares), and compared with the analytical stretched exponential.

IV. FINAL REMARKS

Motivated by the anomalous transport properties of tracer particles diffusing in complex media, particularly of tracers that inherit characteristics of active motion when diffusing in active baths, we propose an extension of active Brownian motion as a model of tracer particles moving in complex media for which the stochastic dynamics of propulsion is driven by scaled Brownian motion, a highly nonstationary process paradigmatic of nonequilibrium stochastic dynamics.

A crossover from ballistic transport in the short-time regime, characteristic of active motion, to genuine anomalous diffusion in the long-time regime with exponent $2 - \beta$ is observed, where β is the exponent that characterizes

sBm. This has been shown from numerical and analytical calculations.

Further, we analyzed the intermediate scattering function $\hat{p}_\beta(\boldsymbol{k},t)$, which corresponds to the Fourier transform of the reduced probability density of finding a particle at position $\boldsymbol{x}$ at time t independent of the direction of propulsion φ, $p_\beta(\boldsymbol{x},t)$. Our numerical analysis shows the discrepancy between the results obtained from the analysis of the ensemble of trajectories generated from Eqs. (5) and the approximation given by Eq. (17); notwithstanding this, the analytical formula for the MSD (21) from such approximation agrees perfectly from our ensemble analysis.

The discrepancy is exhibited in the kurtosis of the particle position distribution $p_\beta(\boldsymbol{x},t)$, mainly in the short-time regime. In this regime, the approximation given by $\hat{q}_\beta^{(1)}$ in Eq. (17) describes coherent transport by the two-dimensional wave equation. This differs from the transport described by the persistence of active motion.

These results are inserted into a wide class of anomalous diffusion systems of tracer particles in nonequilibrium baths, where scaling exponents of the mean-squared displacement in different time regimes vary depending on the specific physical system. The dynamics analyzed in this paper corresponds to systems, described by active Brownian particles, where the stochastic dynamics of the orientational degree of freedom (the particle direction of motion) differs from the dynamics given by thermal fluctuations, in this paper implemented as scaled Brownian motion. Recently, control of the orientational dynamics of active Brownian particles has been achieved through randomly oriented magnetic fields, leading to a rich diffusive behavior [35]. More recently [36], the stochastic dynamics of the orientational degree of freedom of active Brownian particles has been analyzed under the effects of stochastic resetting; this leads to the emergence of interesting spatiotemporal patterns imprinted in an imaginary part of the intermediate scattering function. These recent studies open a direction on the persistent dynamics of active motion.

ACKNOWLEDGMENT

This work was supported by UNAM-PAPIIT IN112623.

APPENDIX: The $\hat{q}_\beta^{\pm 2}$ APPROXIMATION

1. Contribution of $\hat{q}_\beta^{\pm 2}$ to the intermediate scattering function

Consideration of the next Fourier modes, $\hat{q}_\beta^{(\pm 2)}$, to the $\hat{q}_\beta^{(\pm 1)}$ approximation presented in Sec. III A, i.e., disregarding the coefficients $\hat{q}_\beta^{(n)}(\boldsymbol{k},t)$ with $|n|>2$, leads to the following system of coupled equations:

$$\frac{d}{dt}\hat{q}_\beta^{(2)} = -i\frac{v_0}{2}k_- e^{3R_\beta t^\beta}\hat{q}_\beta^{(1)}, \tag{A1a}$$

$$\frac{d}{dt}\hat{q}_\beta^{(1)} = -i\frac{v_0}{2}\left[k_- e^{R_\beta t^\beta}\hat{q}_\beta^{(0)} + k_+ e^{-3R_\beta t^\beta}\hat{q}_\beta^{(2)}\right], \tag{A1b}$$

$$\frac{d}{dt}\hat{q}_\beta^{(0)} = -i\frac{v_0}{2}e^{-R_\beta t^\beta}\left[k_-\hat{q}_\beta^{(-1)} + k_+\hat{q}_\beta^{(1)}\right], \tag{A1c}$$

$$\frac{d}{dt}\hat{q}_\beta^{(-1)} = -i\frac{v_0}{2}\left[k_- e^{-3R_\beta t^\beta}\hat{q}_\beta^{(-2)} + k_+ e^{R_\beta t^\beta}\hat{q}_\beta^{(0)}\right], \tag{A1d}$$

$$\frac{d}{dt}\hat{q}_\beta^{(-2)} = -i\frac{v_0}{2}k_+ e^{3R_\beta t^\beta}\hat{q}_\beta^{(-1)}, \tag{A1e}$$

where we have omitted the arguments for the sake of economy of space and $k_\pm = k_1 \pm ik_2$. By introducing the quantities

$$\hat{J}^{(1)} \equiv ik_-\hat{q}_\beta^{(-1)} + ik_+\hat{q}_\beta^{(1)}, \quad \hat{J}^{(2)} \equiv -k_-^2\hat{q}_\beta^{(-2)} - k_+^2\hat{q}_\beta^{(2)},$$

we can rewrite the system (A1) as

$$\frac{d}{dt}\hat{q}_\beta^{(\mathrm{GTE})} = -\frac{v_0}{2}e^{-R_\beta t^\beta}\hat{J}_\beta^{(1)}, \tag{A2}$$

$$\frac{d}{dt}\hat{J}_\beta^{(1)} = -\frac{v_0}{2}e^{-3R_\beta t^\beta}\hat{J}_\beta^{(2)} + v_0 k^2 e^{R_\beta t^\beta}\hat{q}_\beta^{(\mathrm{GTE})}, \tag{A3}$$

$$\frac{d}{dt}\hat{J}_\beta^{(2)} = \frac{v_0}{2}k^2 e^{R_\beta t^\beta}\hat{J}_\beta^{(1)}, \tag{A4}$$

with $k^2 = k_1^2 + k_2^2$. Notice that by neglecting $\hat{J}_\beta(2)$ from the last system of equations we recover the telegrapher's equation (17), thus $\hat{J}_\beta^{(2)}$ gives the contribution of the Fourier coefficients $\hat{q}_\beta^{(\pm 2)}(\boldsymbol{k},t)$ to the intermediate scattering function.

In Fig. 6 we show a comparison between the ISF obtained from Eq. (17) (dot-dashed lines) and the one obtained from Eq. (A2) (dashed lines) for the case $\beta = 0.4$. For wave vectors smaller than or of the order of the inverse of the length l^{-1}, both approximations give practically the same result [see Figs. 6(a) and 6(b)]. In Fig. 6(a) both approximations are closed to the numerical exact results (open circles), while in Fig. 6(b) they start to depart from the numerical results as kl grows. For $kl = 10.0$ in Fig. 6(c), both approximations depart from the exact result of numerical simulations, but the improvement of the $\hat{q}_\beta^{(\pm 2)}$ approximation over the $\hat{q}_\beta^{(\pm 1)}$ is now clear.

2. No contribution of $\hat{q}_\beta^{(\pm 2)}$ to the second moments of the position distribution

We show in passing that $\hat{q}^{(\pm 2)}$ and higher do not contribute to the second-order moments, thus making the $\hat{q}^{(\pm 1)}$ approximation sufficient to give the exact time dependence of the MSD. The second moment of the ith spatial degree of freedom is

$$\langle x_i^2(t)\rangle_{p_\beta} = -\left[\frac{\partial^2}{\partial k_i^2}\hat{q}_\beta^{(0)}(\boldsymbol{k},t)\right]_{\substack{k_1=0\\k_2=0}}. \tag{A5}$$

We consider the explicit calculation of $\langle x_1^2(t)\rangle$ only, since the calculation of $\langle x_2^2(t)\rangle$ goes on the same line. After taking $\frac{\partial^2}{\partial k_1^2}$ to Eq. (A1c) we have that

$$\frac{d}{dt}\left[\frac{\partial^2}{\partial k_1^2}\hat{q}_\beta^{(0)}\right]_{\substack{k_1=0\\k_2=0}} = -iv_0 e^{-R_\beta t^\beta}\left[\frac{\partial}{\partial k_1}\hat{q}_\beta^{(-1)} + \frac{\partial}{\partial k_1}\hat{q}_\beta^{(1)}\right]_{\substack{k_1=0\\k_2=0}}. \tag{A6}$$

Similarly, by applying $\frac{\partial}{\partial k_1}$ to Eqs. (A1b) and (A1d) we get, respectively,

$$\frac{d}{dt}\left[\frac{\partial}{\partial k_1}\hat{q}_\beta^{(\pm 1)}\right]_{\substack{k_1=0\\k_2=0}} = -i\frac{v_0}{2}e^{-3R_\beta t^\beta}\left[\hat{q}_\beta^{(\pm 2)}\right]_{\substack{k_1=0\\k_2=0}} - i\frac{v_0}{2}e^{R_\beta t^\beta}\left[\hat{q}_\beta^{(0)}\right]_{\substack{k_1=0\\k_2=0}}. \tag{A7}$$

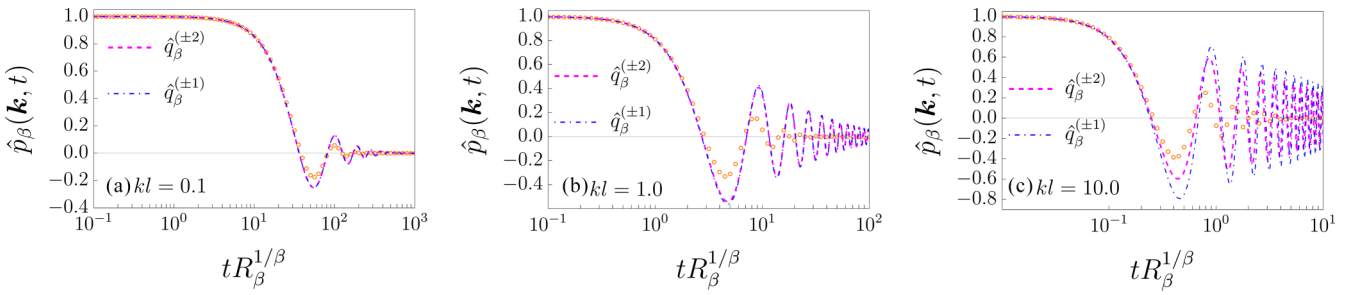

FIG. 6. Comparison of the intermediate scattering function obtained from the $\hat{q}_\beta^{(\pm 2)}$ approximation [$\hat{q}_\beta^{(\mathrm{GTE})}(\boldsymbol{k},t)$ in Eq. (A2), dashed lines]. Dot-dashed lines and open circles correspond to the cases given by the $\hat{q}_\beta^{(\pm 1)}$ approximation from Eq. (17) and by the numerical results obtained from numerical simulations, respectively. Different values of the dimensionless wave vector are shown: $kl = 0.1$ (a), 1.0 (b), and 10.0 (c). In the three cases we have $\beta = 0.4$

Notice that the right-hand side of Eqs. (A1) vanishes when evaluating at $k_1 = 0$ and $k_2 = 0$; thus each $[\hat{q}_\beta^{(n)}]_{\substack{k_1=0\\k_2=0}}$ is stationary whose values correspond to the ones given by the initial conditions, $\delta_{n,0}$ in this case. Therefore, there is no contribution of $\hat{q}_\beta^{(n)}$ with $|n| \leqslant 2$ to the second moment.

We conclude this calculation by noting that

$$\left[\frac{\partial}{\partial k_1}\hat{q}_\beta^{(\pm 1)}\right]_{\substack{k_1=0\\k_2=0}} = -i\frac{v_0}{2}\int_0^t ds\, e^{R_\beta s^\beta}, \tag{A8}$$

and after the substitution of these in Eq. (A6) and the corresponding integration we get

$$\left[\frac{\partial^2}{\partial k_1^2}\hat{q}_\beta^{(0)}\right]_{\substack{k_1=0\\k_2=0}} = -v_0^2\int_0^t ds\, e^{-R_\beta s^\beta}\int_0^s ds_1\, e^{R_\beta s_1^\beta}, \tag{A9}$$

and therefore

$$\langle x_1^2(t)\rangle_{p_\beta} = v_0^2\int_0^t ds\, e^{-R_\beta s^\beta}\int_0^s ds_1\, e^{R_\beta s_1^\beta}. \tag{A10}$$

From here we get

$$\begin{aligned}\langle \boldsymbol{x}^2(t)\rangle_{p_\beta} &= \langle x_1^2(t)\rangle_{p_\beta} + \langle x_2^2(t)\rangle_{p_\beta}\\ &= 2v_0^2\int_0^t ds\, e^{-R_\beta s^\beta}\int_0^s ds_1\, e^{R_\beta s_1^\beta},\end{aligned} \tag{A11}$$

which coincides with the expression given in Eq. (21) obtained from the telegrapherlike Eq. (17) as explained in the text.

3. The contribution of $\hat{q}_\beta^{(\pm 2)}$ to the kurtosis of the position distribution

We now elucidate the contribution of the Fourier modes $\hat{q}_\beta^{(\pm 2)}$ in the fourth moments of $p_\beta(\boldsymbol{x},t)$ given in Eqs. (30). We consider the explicit calculation of $\langle x_1^4(t)\rangle_{p_\beta}$ only since the calculations of $\langle x_2^4(t)\rangle_{p_\beta}$ and $\langle x_1^2(t)x_2^2(t)\rangle_{p_\beta}$ are carried out in the same manner.

Thus after taking $\frac{\partial^4}{\partial k^4}$ of Eq. (A1c) and evaluating it at $k_1 = 0$, $k_2 = 0$ we get

$$\frac{d}{dt}\langle x_1^4(t)\rangle_{p_\beta} = \left[\frac{\partial^4}{\partial k_1^4}\hat{q}_\beta^{(0)}(\boldsymbol{k},t)\right]_{\substack{k_1=0\\k_2=0}} = -2iv_0e^{-R_\beta t^\beta}\left[\frac{\partial^3}{\partial k_1^3}\left(\hat{q}_\beta^{(-1)} + \hat{q}_\beta^{(1)}\right)\right]_{\substack{k_1=0\\k_2=0}}. \tag{A12}$$

The third-order derivatives of $\hat{q}_\beta^{(\pm 1)}$ can be evaluated from Eqs. (A1b) and (A1d):

$$\frac{d}{dt}\left[\frac{\partial^3}{\partial k_1^3}\hat{q}_\beta^{(\pm 1)}\right]_{\substack{k_1=0\\k_2=0}} = -i\frac{v_0}{2}3e^{R_\beta t^\beta}\left[\frac{\partial^2}{\partial k_1^2}\hat{q}_\beta^{(0)}\right]_{\substack{k_1=0\\k_2=0}} - i\frac{v_0}{2}3e^{-3R_\beta t^\beta}\left[\frac{\partial^2}{\partial k_1^2}\hat{q}_\beta^{(\pm 2)}\right]_{\substack{k_1=0\\k_2=0}}, \tag{A13}$$

where the last term gives the contribution of $\hat{q}_\beta^{(\pm 2)}$ to the fourth moment $\langle x_1^4(t)\rangle_{p_\beta}$. The second derivative of $\hat{q}_\beta^{(0)}$ is already given in Eq. (A9). The second derivatives of $\hat{q}_\beta^{(\pm 2)}$ are computed from Eqs. (A1a) and (A1e):

$$\frac{d}{dt}\left[\frac{\partial^2}{\partial k_1^2}\hat{q}_\beta^{(\pm 2)}\right]_{\substack{k_1=0\\k_2=0}} = -i\frac{v_0}{2}e^{3R_\beta t^\beta}\left[\frac{\partial}{\partial k_1}\hat{q}_\beta^{(\pm 1)}\right]_{\substack{k_1=0\\k_2=0}}, \tag{A14}$$

where the last factor in the right-hand side is already given in Eq. (A8). From these results we get

$$\left[\frac{\partial^2}{\partial k_1^2}\hat{q}_\beta^{(\pm 2)}\right]_{\substack{k_1=0\\k_2=0}} = -\frac{v_0^2}{2}\int_0^t ds\, e^{3R_\beta s^\beta}\int_0^s ds_1 e^{R_\beta s_1^\beta}. \tag{A15}$$

All these results put together allow the integration of Eq. (A13) that gives

$$\left[\frac{\partial^3}{\partial k_1^3}\hat{q}_\beta^{(\pm1)}\right]_{\substack{k_1=0\\k_2=0}} = 12i\left(\frac{v_0}{2}\right)^3\int_0^t ds e^{R_\beta s^\beta}\int_0^s ds_1 e^{-R_\beta s_1^\beta}\int_0^{s_1} ds_2 e^{R_\beta s_2^\beta} + 6i\left(\frac{v_0}{2}\right)^3\int_0^t ds e^{-3R_\beta s^\beta}\int_0^s ds_1 e^{3R_\beta s_1^\beta}\int_0^{s_1} ds_2 e^{R_\beta s_2^\beta}. \tag{A16}$$

Correspondingly, after substitution of this in Eq. (A12) and integrating we have that the fourth moment of the coordinate x_1 (the other gives the same result) is

$$\begin{aligned}\left\langle x_1^4(t)\right\rangle_{p_\beta} &= 6v_0^4\int_0^t ds e^{-R_\beta s^\beta}\int_0^s ds_1 e^{R_\beta s_1^\beta}\int_0^{s_1} ds_2 e^{-R_\beta s_2^\beta}\int_0^{s_2} ds_3 e^{R_\beta s_3^\beta}\\ &+ 3v_0^4\int_0^t ds e^{-R_\beta s^\beta}\int_0^s ds_1 e^{-3R_\beta s_1^\beta}\int_0^{s_1} ds_2 e^{3R_\beta s_2^\beta}\int_0^{s_2} ds_3 e^{R_\beta s_3^\beta},\end{aligned} \tag{A17}$$

the second term in the right-hand side being the contribution due to $\hat{q}_\beta^{(\pm2)}$. By a similar procedure we obtain for $\langle x_1^2(t)x_2^2(t)\rangle_{p_\beta}$

$$\begin{aligned}\left\langle x_1^2(t)x_2^2(t)\right\rangle_{p_\beta} &= 2v_0^2\int_0^t ds e^{-R_\beta s^\beta}\int_0^s ds_1 e^{R_\beta s_1^\beta}\int_0^{s_1} ds_2 e^{-R_\beta s_2^\beta}\int_0^{s_2} ds_3 e^{R_\beta s_3^\beta}\\ &+ v_0^4\int_0^t ds e^{-R_\beta s^\beta}\int_0^s ds_1 e^{-3R_\beta s_1^\beta}\int_0^{s_1} ds_2 e^{3R_\beta s_2^\beta}\int_0^{s_2} ds_3 e^{R_\beta s_3^\beta}.\end{aligned} \tag{A18}$$

Substituting Eqs. (A17) and (A18) into Eq. (29), and considering that $\langle x_1^4(t)\rangle_{p_\beta} = \langle x_2^4(t)\rangle_{p_\beta}$, we have that in the $\hat{q}_\beta^{(\pm2)}$ approximation $\kappa_\beta(t)$ can be written as $\kappa_\beta(t) = \kappa_{\beta,\mathrm{TE}}(t) + \kappa_\beta^{(2)}(t)$ where the contribution of $\hat{q}_\beta^{(\pm2)}$ to the kurtosis is given by

$$\kappa_\beta^{(2)}(t) = 8\frac{\int_0^t ds\, e^{-R_\beta s^\beta}\int_0^s ds_1\, e^{-3R_\beta s_1^\beta}\int_0^{s_1} ds_2\, e^{3R_\beta s_2^\beta}\int_0^{s_2} ds_3\, e^{R_\beta s_3^\beta}}{\left[\int_0^t ds\, e^{-R_\beta s^\beta}\int_0^s ds_1\, e^{R_\beta s_1^\beta}\right]^2}. \tag{A19}$$

The leading time dependences for the numerator and denominator in the short-time regime of the last expression are, respectively, $t^4/24$ and $t^4/4$, with which along with the result of Sec. III C, $\kappa_{\beta,\mathrm{TE}} = \frac{8}{3}$, we get $\kappa_\beta = \frac{8}{3} + \frac{4}{3} = 4$, thus recovering the exact results from numerical simulations $\kappa_\beta = 4$ as is shown in Fig. 4. This calculation elucidates the role of the Fourier coefficients $\hat{q}_\beta^{(\pm2)}$.

[1] X.-L. Wu and A. Libchaber, Phys. Rev. Lett. **84**, 3017 (2000).
[2] H. Kurtuldu, J. S. Guasto, K. A. Johnson, and J. P. Gollub, Proc. Natl. Acad. Sci. USA **108**, 10391 (2011).
[3] K. Kanazawa, T. G. Sano, A. Cairoli, and A. Baule, Nature (London) **579**, 364 (2020).
[4] S. Thapa, N. Lukat, C. Selhuber-Unkel, A. G. Cherstvy, and R. Metzler, J. Chem. Phys. **150**, 144901 (2019).
[5] X. Cao, B. Zhang, and N. Zhao, Mol. Phys. **118**, e1730992 (2020).
[6] H. Vandebroek and C. Vanderzande, Phys. Rev. E **92**, 060601(R) (2015).
[7] H. Vandebroek and C. Vanderzande, J. Stat. Phys. **167**, 14 (2017).
[8] C. Yuan, A. Chen, B. Zhang, and N. Zhao, Phys. Chem. Chem. Phys. **21**, 24112 (2019).
[9] J. R. Gomez-Solano and F. J. Sevilla, J. Stat. Mech.: Theory Exp. (2020) 063213.
[10] S. C. Lim and S. V. Muniandy, Phys. Rev. E **66**, 021114 (2002).
[11] F. Thiel and I. M. Sokolov, Phys. Rev. E **89**, 012115 (2014).
[12] J.-H. Jeon, A. V. Chechkin, and R. Metzler, Phys. Chem. Chem. Phys. **16**, 15811 (2014).
[13] H. Safdari, A. G. Cherstvy, A. V. Chechkin, F. Thiel, I. M. Sokolov, and R. Metzler, J. Phys. A **48**, 375002 (2015).
[14] G. K. Batchelor, Math. Proc. Camb. Philos. Soc. **48**, 345 (1952).
[15] E. B. Postnikov and I. M. Sokolov, Physica A **391**, 5095 (2012).
[16] G. Guigas, C. Kalla, and M. Weiss, Biophys. J. **93**, 316 (2007).
[17] N. V. Brilliantov and T. Pöschel, Phys. Rev. E **61**, 1716 (2000).
[18] M. J. Saxton, Biophys. J. **81**, 2226 (2001).
[19] J. Wu and K. M. Berland, Biophys. J. **95**, 2049 (2008).
[20] H. Safdari, A. G. Cherstvy, A. V. Chechkin, A. Bodrova, and R. Metzler, Phys. Rev. E **95**, 012120 (2017).
[21] V. Sposini, R. Metzler, and G. Oshanin, New J. Phys. **21**, 073043 (2019).
[22] M. A. dos Santos and L. M. Junior, Chaos, Solitons, and Fractals **144**, 110634 (2021).
[23] A. S. Bodrova, A. V. Chechkin, and I. M. Sokolov, Phys. Rev. E **100**, 012120 (2019).
[24] A. S. Bodrova, A. V. Chechkin, and I. M. Sokolov, Phys. Rev. E **100**, 012119 (2019).
[25] V. Stojkoski, T. Sandev, L. Kocarev, and A. Pal, Phys. Rev. E **104**, 014121 (2021).
[26] A. S. Bodrova, A. V. Chechkin, A. G. Cherstvy, and R. Metzler, New J. Phys. **17**, 063038 (2015).
[27] A. Valdés Gómez and F. J. Sevilla, Phys. Rev. E **108**, 054117 (2023).

[28] B. ten Hagen, S. van Teeffelen, and H. Löwen, J. Phys.: Condens. Matter **23**, 194119 (2011).
[29] F. J. Sevilla and L. A. Gómez Nava, Phys. Rev. E **90**, 022130 (2014).
[30] C. Kurzthaler, S. Leitmann, and T. Franosch, Sci. Rep. **6**, 36702 (2006).
[31] C. Kurzthaler and T. Franosch, Soft Matter **13**, 6396 (2017).
[32] S. I. Heizler, Nucl. Sci. Eng. **166**, 17 (2010).
[33] F. J. Sevilla and M. Sandoval, Phys. Rev. E **91**, 052150 (2015).
[34] K. V. Mardia, Sankhyā: The Indian Journal of Statistics, Series B **36**, 115 (1974).
[35] M. A. Fernandez-Rodriguez, F. Grillo, L. Alvarez, M. Rathlef, I. Buttinoni, G. Volpe, and L. Isa, Nat. Commun. **11**, 4223 (2020).
[36] Y. Baouche, T. Franosch, M. Meiners, and C. Kurzthaler, Active Brownian particle under stochastic orientational resetting, arXiv:2405.06769.